Microelectronics Reliability 100–101 (2019) 113362

Contents lists available at ScienceDirect

Microelectronics Reliability

journal homepage: www.elsevier.com/locate/microrel

Analysis of electromigration failure of nano-interconnects through a combination of modeling and experimental methods

H. Ceric[a,*], H. Zahedmanesh[b], K. Croes[b]

[a] Institute for Microelectronics, TU Wien, Austria
[b] imec, Leuven 3001, Belgium

A B S T R A C T

Electromigration assessment and optimization of nano-interconnects is a complex task which ultimately demands an application of both experimental and modeling methods. The goal of this work is to introduce and discuss a modeling concept that is not unnecessarily complex and that can be optimally combined with experimental studies in order to assess the relative impact of different factors on interconnect reliability. The presented model and related modeling methodology are applied to a set of electromigration tests.

1. Introduction

Over the past decades, the electromigration (EM) reliability of on-chip Cu wiring in the back end of the line (BEOL) has been a long-standing concern for the development of devices with high density and performance. The multitude of impact factors determining the development of EM failure and interconnect lifetime [1] demands a close exchange between experimental and modeling methods. From the very beginning of EM investigation, different types of modeling approaches have been utilized to describe and understand the degradation phenomena and to predict lifetime of interconnect structures affected by EM. As interconnect technology moves to the nano-scale, changes in the basic technology produce a need for updated EM models. There are three principal challenges in the modeling of nano-scaled interconnects.

The first challenge involves the layout of the studied interconnect structure. In order to reproduce realistic mechanical conditions, all materials in the layout and their corresponding properties need to be included in the overall modeling framework. Only with this comprehensive approach the mechanical effect of low-*k* materials can be considered.

The second challenge is the physics of grain boundaries (GBs) and interfaces that can be modeled with different levels of complexity, either by applying dedicated local sub-models or by using cumulative and average values. Interconnect scaling has led to significant changes in the microstructure of the Cu line where the polycrystalline sections increasingly dominate large portions of the interconnect length [2,3]. As the thickness of interconnects decreases, the importance of EM-induced mass transport along GBs and interfaces increases.

The third challenge is the modeling of void growth, which leads to an increase in interconnect resistance and to its final failure, at the necessary level of accuracy. In down-scaled interconnect, smaller voids are necessary in order to produce the fatal failure and the dynamics of void growth strongly depends on the local microstructural features.

The goal of the work presented in this paper is to meet the above mentioned challenges by a comprehensive modeling methodology (Section 2) and to apply it for a comparative study of the failure behavior of a specific interconnect layout.

Particular emphasis has been put on the investigation of the causes of bi-modal character of the failure (Section 3). Attained insights have been used to draft a modeling methodology which is applied for predictive simulations (Section 4).

2. Models used for simulation

The development of EM failure goes through two distinctive phases: void nucleation phase and void evolution phase. According to the usual modeling approach, the lifetime of an interconnect structure, t_f, consists of a void nucleation, t_N, and void evolution time, t_E, corresponding to two failure development phases,

$$t_f = t_N + t_E. \quad (1)$$

Each of these two phases demands its own modeling approach, that is why we are talking about *void nucleation* and *void evolution* model.

2.1. Vacancy migration

In the pioneering work by Sarychev, Zithnikov et al. [4], the general framework for EM degradation modeling of metallic interconnects in

* Corresponding author.
E-mail address: ceric@iue.tuwien.ac.at (H. Ceric).

https://doi.org/10.1016/j.microrel.2019.06.054
Received 15 May 2019; Accepted 21 June 2019
Available online 23 September 2019

microscaled regions is provided. Since then, the original model has been extended and refined to include treatment of various microstructural properties of metal and interfaces, such as crystal anisotropy, stress-dependent diffusivities, etc. [5].

The central governing equations of EM models are the vacancy flux (2) and vacancy balance Eq. (3):

$$\vec{J_v} = \boldsymbol{D}_{\text{eff}}\left(\frac{C_v}{kT}\,|Z^*_{\text{eff}}e|\,\rho\vec{j} + \frac{C_v}{kT} f\Omega\nabla p - \nabla C_v\right), \tag{2}$$

$$\frac{\partial C_v}{\partial t} = -\nabla\cdot\vec{J_v} + G_{\text{eff}}(C_v), \tag{3}$$

where C_v is the vacancy concentration, p is the hydrostatic stress, ρ is the interconnect resistivity, $\vec{j}$ is the current density, Ω is the atomic volume, and f is the atom-vacancy relaxation factor. G_{eff} is the Rosenberg-Ohring recombination term and Z_{eff}^* is the effective valence which are discussed in detail in Section 2.5. One of the most important differences between the vacancy flux defined in (2) and the flux in the original Sarychev, Zithnikov et al. [4] paper is the diffusivity tensor, $\mathbf{D}_{\text{eff}}$, which describes an anisotropy of vacancy transport caused by the crystal deformation [5].

The dynamics of vacancy flux, $\vec{J_v}$, plays a crucial role in the development of EM failure. When for $\vec{J_v} = 0$, the stress equilibrium state is achieved (cf. Fig. 1), for a back-flow stress which is lower than the critical stress-threshold needed for void nucleation, the interconnect is virtually "immortal" (arbitrarily long-lived). This situation corresponds to Blech's effect in 1D and it is its actual generalization. Blech's condition directly follows from the zero-flux condition ($\vec{J_v} = 0$) if we assume that the pressure and vacancy concentration are in a local equilibrium [6],

$$C_v = C_v^0 \exp\left(W_f - \frac{\Omega p}{kT}\right), \tag{4}$$

where W_f is the interaction energy between the vacancy and the stress field and C_v^0 is the vacancy concentration in the absence of any stress effects. Inserting (4) into (2) for $\vec{J_v} = 0$ we obtain for a 1D linear interconnect of the length l,

$$j_x l = \frac{\Omega(1+f)\Delta\sigma_x^{\text{eq}}}{\rho\,|Z^*_{\text{eff}}e|} = \frac{\Omega(1+f)|\sigma_x(l) - \sigma_x(0)|}{\rho\,|Z^*_{\text{eff}}e|}, \tag{5}$$

where $p = -\sigma_x$ and $\sigma_x(l)$ and $\sigma_x(0)$ are stresses at the both ends of the linear interconnect.

When the zero-flux condition is attained for a certain back-stress which is higher than the critical-stress needed for void nucleation, a void embryo is formed.

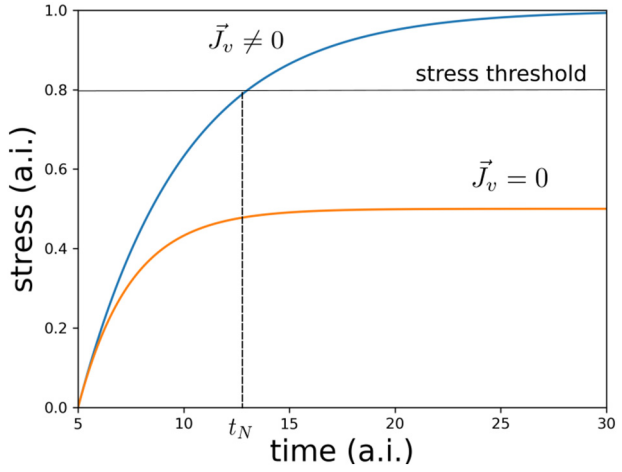

Fig. 1. Stress dynamics in dependence of zero-flux condition.

2.2. Mechanics

Both the void nucleation, as well as the void evolution model, are solved simultaneously with the equations of mechanical model [5]:

$$\frac{\partial\varepsilon_{ij}^v}{\partial t} = \frac{1}{3}\Omega\left[((1-f)\nabla\cdot\vec{J_v} + fG_{\text{eff}}(C_v)]\delta_{ij}.\right. \tag{6}$$

$$\nabla\cdot\sigma = \mathbf{0}, \quad \sigma = \mathbf{E}(\varepsilon - \varepsilon^v - \varepsilon^{th}) + \sigma_0. \tag{7}$$

Here $\mathbf{E}$ is the fourth-order elasticity tensor. ε^v is the volumetric strain component which rises due to EM and ε^{th} represents an impact of thermal loads.

From the stress tensor, σ, the normal stresses at all interfaces and GBs can be obtained. The *void nucleation phase* ends when one of these normal stresses surmounts the local critical stress-threshold.

2.3. Void nucleation

The conditions for void nucleation are established either due to geometrical or microstructural features of interconnect metal and layout. A particular geometrical feature can cause an interruption of a vacancy flux and local accumulation of vacancy concentration which leads to the local increase of tensile mechanical stress. After a certain stress-threshold is attained an initial void is nucleated [7]. A microstructural feature like grain boundary can also lead to the local disturbance of mass transport and subsequent rise of tensile stress at the so-called triple-points (intersection of GB with interface). After an initial void is formed, the previously built stress relaxes. The volume of the initial void is determined as:

$$V_0 = -\frac{1}{B}\int_V p(x,y,z)\,dx\,dy\,dz. \tag{8}$$

Here $p(x,y,z)$ is the pressure distribution inside the interconnect at the moment when the critical stress is reached and B the effective modulus [7]. In order to simplify the model's implementation, it is assumed that a cylindrical void with is formed around the triple-point and spans the entire interconnect width, w. This assumption allows for the calculation of the initial void radius, r_0:

$$r_0 = \sqrt{\frac{2V_0}{\pi w}}. \tag{9}$$

2.4. Void evolution

In order to estimate a duration of the second phase of failure development, it is necessary to model the void growth velocity v_n. The normal velocity, v_n, of the void surface is calculated according to [5].

$$v_n = \Omega(\vec{J_v}\cdot\vec{n} - \nabla\cdot\vec{J_s}). \tag{10}$$

From (10) it can be seen that the void surface evolves due to the vacancy transport in the normal direction, $\vec{J_v}\cdot\vec{n}$, and the divergence of the surface vacancy flux, $\nabla\cdot\vec{J_s}$. The surface vacancy flux itself, $\vec{J_s}$, rises due to the tangential component of the current density, $\vec{j_t}$, and the surface gradient of the chemical potential μ_s

$$\vec{J_s} = -\frac{D_s\delta_s}{kT\Omega}(|Z_s^*e|\,\rho\vec{j_t} + \nabla_s\mu_s), \tag{11}$$

where D_s is the surface diffusivity and δ_s is the thickness of the diffusion layer. The surface chemical potential, μ_s, is given as

$$\mu_s = \Omega(W_s - \gamma_s\kappa), \tag{12}$$

where γ_s is the surface energy, κ is the local curvature of the surface and $W_s = (\sigma:\varepsilon)/2$ is the local elastic strain density. By further assuming that the void not only begins as a half-cylinder but that it also remains in this shape throughout its growth, the calculations (10), (11), and (12), can

be significantly simplified (e.g. $\nabla_s \kappa = 0$) and the relationship $v_n = v_n(r)$ established. The void evolution time, t_E, is obtained by integration:

$$t_E = \int_{r_0}^{r_c} \frac{dr}{v_n^{\max}(r)}. \tag{13}$$

For the integral evaluation, the worst case scenario is assumed, i.e., the whole void surface moves with a maximum velocity $v_n{}^{\max}$ calculated on its surface. Here, the critical void radius, r_c, is the solution of the equation

$$R_{\text{failure}} = R_{\text{total}}(r_c). \tag{14}$$

2.5. Effective values

The crucial parameter for an estimation of the effective values for diffusivities, effective valences, and recombination times for interconnect metal containing a network of GBs embedded in different types of interface layers is the volume fraction, ϵ, of GBs in the metal body. This parameter can be estimated by Smith's theory [8], from SEM/TEM pictures or by means of microstructural simulation [9].

The volume fraction dependent effective values of the Rosenberg-Ohring term, G_{eff}, the effective valence, Z_{eff}^*, and the effective diffusivity, D_{eff}, are given by the following terms, respectively:

$$G_{\text{eff}}(C_v) = -(C_v^0 - C_v)\left(\frac{1-\epsilon}{\tau_{bulk}} + \frac{\epsilon}{\tau_{gb}}\right), \tag{15}$$

$$Z_{\text{eff}}^* = Z_{\text{bulk}}^*(1-\epsilon) + Z_{\text{gb}}^*\epsilon, \tag{16}$$

$$D_{\text{eff}} = D_{\text{bulk}} + D_{\text{lin}}\left(\frac{2}{w} + \frac{1}{h}\right)\delta_{\text{I-lin}} + D_{\text{cap}}\frac{\delta_{\text{I-cap}}}{h} + \epsilon D_{\text{gb}}, \tag{17}$$

where h is the interconnect thickness and w is the interconnect width. Each of the transport paths is characterized by its diffusivity and its thickness: bulk (D_{bulk}, h), capping layer ($D_{\text{cap}}, \delta_{\text{I-cap}}$), and liner ($D_{\text{lin}}$, $\delta_{\text{I-lin}}$). The GBs are characterized by their diffusion coefficient and the GB volume fraction, ϵ: (D_{gb}, ϵ).

τ_{bulk} and τ_{gb} ($\tau_{\text{bulk}} \ll \tau_{\text{gb}}$) are vacancy recombination times in the bulk and GBs respectively.

The bulk effective valence, Z_{bulk}^*, and resistivity, ρ, are related on the fundamental level since both of these parameters characterize different aspects of electron scattering in a current carrying metal,

$$Z_{\text{bulk}}^*(T) = Z_d + Z_w(T) = Z_d + \frac{K}{\rho(T)}. \tag{18}$$

Here Z_d is the direct valence which is assumed to be equal to the bare valence of Cu. K is the proportionality factor which has been fitted for Z_{bulk} for the thick interconnect at the room temperature.

Different advanced models can be used for the modeling of interconnect resistivity [10]. In reference to [11], for the value of the effective valence in GBs, an estimate $Z_{\text{gb}}^* \approx 0.8 Z_{\text{bulk}}^*$, is used.

2.6. Grain boundary model

In order to capture mechanism of void nucleation at a triple-point, more detailed modeling than provided by expressions (15), (16), and (17) is necessary. The corresponding model was derived in [12]:

$$J_{v,1} = \omega_T(C_v^{\text{eq}} - C_v^{\text{im}})C_{v,1} - \omega_R C_v^{\text{im}}, \tag{19}$$

$$-J_{v,2} = \omega_T(C_v^{\text{eq}} - C_v^{\text{im}})C_{v,2} - \omega_R C_v^{\text{im}}. \tag{20}$$

The model describes trapping and release of vacancies inside a grain boundary with the rates ω_T and ω_R, respectively. The trapped vacancies, from both sides of the grain boundary become immobile vacancies with corresponding concentration $C_v{}^{\text{im}}$. The relationship between the GB model (defined by (19) and (20)) and the Rosenberg-Ohring term (15) is discussed in [5]. The parameters ω_T and ω_R can ultimately be determined only by means of molecular dynamics. For the purpose of this study they are set in such a way that the condition for void nucleation at the triple-point is fulfilled.

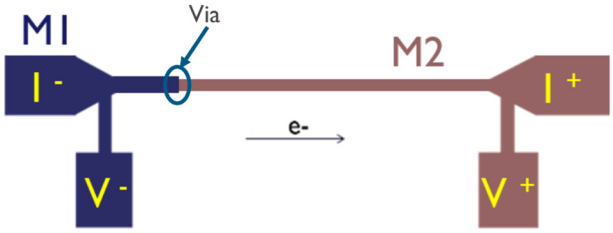

Fig. 2. Test structure consists of M1 and M2 metallization and the via. [13].

From (19) and (20) the original Rosenberg-Ohring term can be derived [12]:

$$G_{\text{gb}} = \frac{1}{\tau_{\text{gb}}}\left(C_v^{\text{eq}} - C_v^{\text{im}}\left(1 - \frac{2\omega_R}{\omega_T(C_{v,1} + C_{v,2})}\right)\right) \tag{21}$$

$$\tau_{\text{gb}} = \frac{\delta}{\omega_T(C_{v,a} + C_{v,2})} \tag{22}$$

By choosing $\omega_T(C_{v,\,1} + C_{v,\,2}) \gg 2\omega_R$ expression (21) reduces to the Rosenberg-Ohring term.

Besides the described model, also a function of GB as a fast diffusivity path needs to be considered. This is done by setting D_{gb} into the geometrical plane separating two grains. Fluxes (19) and (20) regulate vacancy transport through this plane.

3. Experimental and simulative settings

The test structure shown in Fig. 2 consists of 170 μm long and 23 nm wide Cu M2-line connected to 80 nm wide M1-feeder line [13]. The microstructures of the Cu lines were examined by the transmission electron micrographs. Bamboo-like, near-bamboo, and polycrystalline structures were found in the M2 line. The samples were tested in a vacuum furnace at temperatures ranging from 230°C, 280°C, and 330°C with a current density of 1.68MA/cm^2 through the via. Once the line resistance change $\Delta R/R$ becomes equal to or greater than 20% the test for that line was terminated.

3.1. Analysis of experimental results

The most striking feature of the experimental results in the focus is the bi-modality of the failure (see Fig. 3). TD-SEM pictures clearly show (see [13] for more details) that the early failure occurs due to the void nucleation in the via at the end of the line (Mode I) and late failure (Mode II) due to the void in the line (M2) itself. Regarding microstructure, study of TD-SEM pictures reveals a very uneven distribution

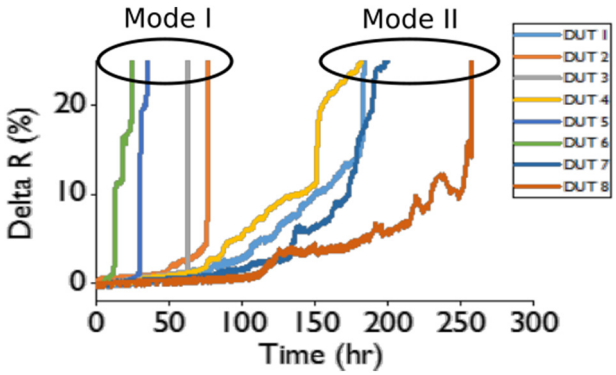

Fig. 3. Time-resistance curves for 230 °C [13]. The tested samples show bimodal behavior.

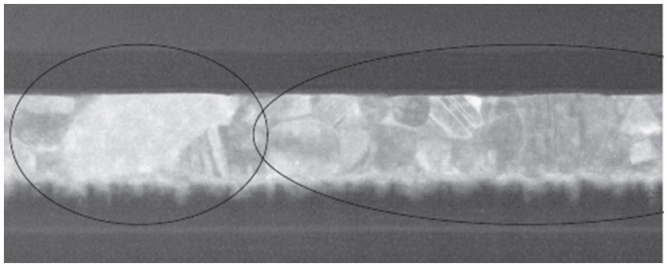

Fig. 4. TD-SEM picture of interconnect's microstructure [14].

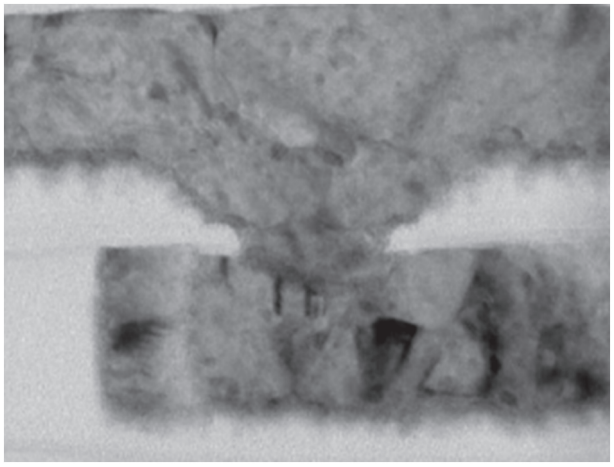

Fig. 5. TD-SEM picture of the microstructure in the via [14].

of grain sizes. Polycrystalline regions are interrupted by a single, larger grain (c.f. Fig. 4).

If we take a closer look on the position of the nucleated voids, we frequently find that voids are nucleated inside a larger grain. However, most failures are observed in the via itself (Mode I). Via clearly represents an obstacle to the mass transport and, with or without any microstructure, it is prone for development of fatal void. Typically, vias are filled with 2–3 larger grains (c.f. Fig. 5). The detailed structure of the layer including Cu line, cap and barrier layer is presented in Fig. 6.

3.2. Choosing a model for simulation

On the basis of analysis of experimental results from the previous section we define two tasks for modeling and simulation:

1. Explanation of the failure's bi-modal feature.
2. Prediction of lifetimes at 280 °C and 330 °C using the model calibrated at 230 °C.

The working hypothesis is that peak stresses are reached at the bottom of the via and at some triple-point connected to a larger grain in the M2 line. As a possible, decisive, impact factor determining the

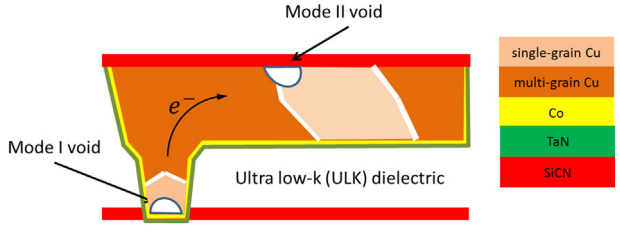

Fig. 6. Structure used for simulations. Cylindrical void nucleation is assumed at the triple-point for Mode II failure.

Table 1
Mechanical properties [7].

Layer	Young modulus (GPa)	Poisson coeff.
Cu bulk	117	0.30
Co liner	207	0.31
TaN liner	186	0.36
SiCN capping	100	0.24
ULK (2.5)	9	0.20

failure's mode is the grain size of the large grain in the M2 line. In other words a certain grain size can lead to the faster rise of stress at the nearby triple-point than at the via's bottom. Modeling of vacancy flux and mechanical stress in each single grain and at the GBs is possible but it would be a time-consuming venture, particularly if, for the sake of accuracy, we need to include in the simulation as large portions of interconnect's layout as possible. To reconcile these demands, and with regard to the two tasks defined above, we choose to describe the portions with finer grains by utilizing the effective values (Section 2.5) and to simulate GBs of the larger grains with a detailed model (Section 2.6). The basic layout used for the simulation is presented in Fig. 6. Mechanical parameters and diffusion coefficients used for simulation are given in Tables 1 and 2.

Pre-exponentials for SiCN, Cu GBs, and Cu surface are not found in the literature. In the reference to the Cu bulk value they are set to 10^{-5} m^2/s. Mass transport along Co liner has been neglected.

4. Comparative studies

In order to estimate interconnect lifetime (t_F), both void nucleation (t_N), as well as the void evolution time (t_E), need to be estimated as accurately as possible. In its simplest form, an estimation of t_N demands that Eqs. (2), (3), (6), and (7) be solved simultaneously. The same group of equations needs to be solved for the interconnect containing a void in order to determine the function $v_n(r)$ and subsequently to estimate t_E by the integral (13). COMSOL Multiphysics [18] was used for the simulations.

The capping layer (SiCN) and liner (Co/TaN) are implemented using COMSOL-shell model, the whole structure is embedded in a box of dielectric. All dimensions, materials, and material properties are set in accordance to the experimental configuration (Section 3.1 and Figs. 6 and 7).

4.1. Failure bi-modality

According to our working assumptions, during the simulation, the stress component normal to the via bottom (Mode I) and the normal stress component normal to the Cu/capping interface at the triple-point connected to a large grain in the line (Mode II) were monitored. In Fig. 7 an example of the structure used for simulations is presented. Both Grain 1 and Grain 2 domains are meshed with a finer mesh in order to obtain accurate values of the stresses at the via bottom and at the triple-point. In order to determine a possible cause for the failure bimodality we gradually change the volume of the Grain 2 and at the same time monitor how the peak stress changes at the triple-point belonging to the Grain 2. For the smaller Grain 2 volumes, stress reached

Table 2
Diffusion coefficients.

Layer	Pre-exponential (m^2/s)	Act. energy (eV)
Cu bulk	7.8×10^{-5} [15]	2.2 [15]
SiCN	NA	0.9 [7]
Cu GBs	NA	0.8 [16]
Cu surface	NA	0.7 [17]

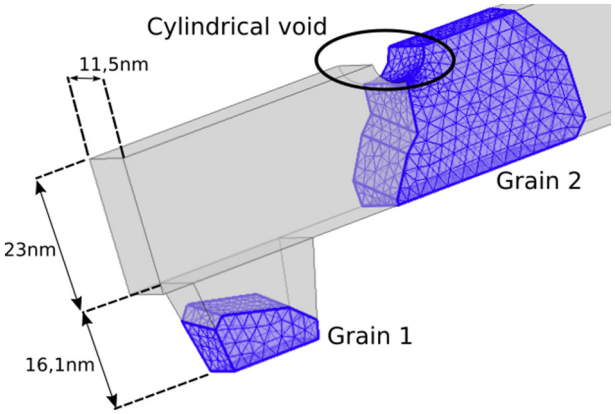

Fig. 7. Grain 1 at the bottom of the via and Grain 2 inside the M2 line. The embryo of cylindrical void with radius r_0 (see (9)) is placed at the triple-point where stress-threshold is reached.

at the bottom of the via and inside the Grain 1 is not only higher but it also grows faster. The situation changes when the volume of the Grain 2 reaches a certain threshold size in which case we observe a higher stress dynamics at the triple-point belonging to the Grain 2. These simulation results support the original assumption that the bi-modality of EM failure rises due to this specific feature of the microstructure. In the considered cases (cf. Fig. 7), due to the current direction, geometry alone cannot be the cause of the Mode II failure. The size of the large grain, lying directly in the M2 line, reveals itself as the main cause.

4.2. Reproducing the experimental results

In the calibration process a chosen set of model parameters is adjusted in order that simulation accurately reproduce average interconnect lifetime for 230 °C. The parameters essential for the failure dynamics are activation energies for Cu-bulk, cap, liner, and GBs and the corresponding pre-exponentials for diffusivity Arrhenius's law. Parameters chosen for calibration are Arrhenius's law pre-exponentials for GB diffusion ($D_{\mathrm{GB}}{}^0$) and diffusion along void surface ($D_s{}^0$), needed for void evolution model and an estimation of the void evolution (growth) time t_E (Section 2.4). The corresponding activation energies are obtained from the published results (see Table 2). After fitting procedure is performed the following values are obtained

$$D_{\mathrm{GB}} = 3.1 \times 10^{-3} \exp\left(-\frac{0.8\mathrm{eV}}{kT}\right)\left[\frac{m^2}{s}\right], \tag{23}$$

for the average grain size of 5 nm (in the polycrystalline sections of the interconnect line) and

$$D_s = 0.12 \exp\left(-\frac{0.7\mathrm{eV}}{kT}\right)\left[\frac{m^2}{s}\right]. \tag{24}$$

for the surface diffusivity. While values of activation energies for different migration paths are abundantly available in the literature there is to our best knowledge no such information for pre-exponentials. Some related research [15,19] indicates that $D_{\mathrm{GB}}{}^0$ is more than 100 times lower than the value presented in (23). As the next step in the research will also include the statistics of Cu line microstructure, it is to be expected that pre-exponential values will be further adjusted.

4.3. Predictive simulations

Determining stress-threshold needed for void nucleation is of crucial importance (Section 2.3). Here we rely on the model developed at IMEC and calibrated to the experimental results [7] which allows us to estimate stress-threshold for SiCN: $\sigma_{\mathrm{th}}(230°\mathrm{C}) = 201.77\mathrm{MPa}$ and $\sigma_{\mathrm{th}}(230\,°\,\mathrm{C})\mathrm{MPa}$. At 330 °C the stress-threshold is very low, almost zero.

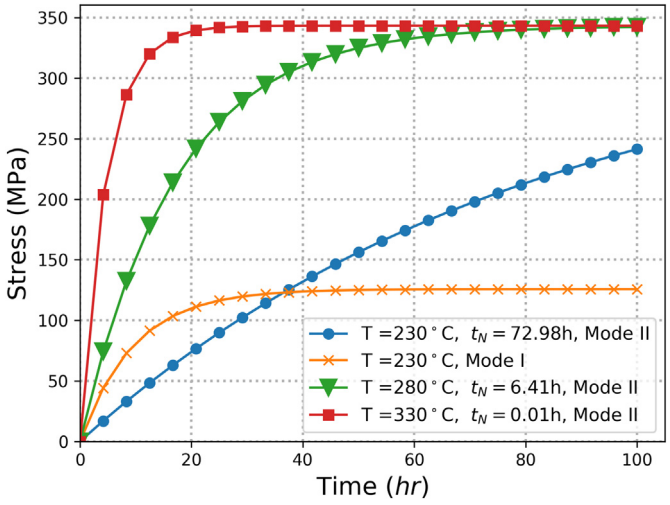

Fig. 8. Stress-time dynamics for Mode I and Mode II failure sites. The stress-threshold is reached at the triple-point belonging to the large grain in the M2 line that corresponds to the Mode II failure.

At this temperature, due to thermomechanics, the initial stress in the interconnect line is compressive.

With the model calibrated at 230 °C the interconnect lifetimes at temperatures 280 °C and 330 °C are estimated by simulations (c.f. Fig. 8). As we can see in Table 3, the average lifetimes (t_f) are predicted with a moderate error. Having in mind the procedure applied for the simulative estimation of lifetimes, it seems straightforward, that the results can be further improved by including statistics of large grain sizes and positions into the model.

5. Conclusion and outlook

In this paper we applied a comprehensive, physically based, modeling of EM degradation in order explain bi-modality of the failure behavior and to assess the capability of the model to predict interconnect's lifetime for two different temperatures. Obtained simulation results imply that the possible reason for an occurrence of Mode II is the presence of grains in the M2 line larger than a certain grain size threshold. The differences between the lifetimes predicted by the simulation and the measured lifetime suggests that, while the proposed model has a clear potential to be a useful tool for reliability assessment, there is a still work to be done both at the model itself as well at the calibration and simulation methodology.

Declaration of Competing Interest

The authors declare that they have no known competing financial interests or personal relationships that could have appeared to influence the work reported in this paper.

Table 3
Comparison between experimental t_f^{exp} and simulated t_f average Mode II failure times.

T [°C]	t_N [h]	t_E [h]	t_f [h]	t_f^{exp} [h]	err [%]
230	**72.98**	**74.41**	**147.49**	**147.49**	**0.0**
280	6.41	20.84	27.25	21.93	24.26
330	0.01	7.70	7.71	6.53	18.7

The times denoted in bold font in the first row of the table, t_N, t_E, and t_f, are extracted from the experiments performed at 230 °C (see Fig. 8).
These experimentally determined times are used for model calibration and for estimation of t_N, t_E, and t_f at 280 °C and 330 °C.

References

[1] Z. Tőkei, End of Cu Roadmap and Beyond Cu, Invited talk at IEEE Proc. Intl. Interconn. Techn. Conf., 2016.

[2] S. Choi, C. Christiansen, L. Cao, J. Zhang, R. Filippi, T. Shen, K.B. Yeap, S. Ogden, H. Zhang, B. Fu, P. Justison, Effect of metal line width on electromigration of BEOL Cu interconnects, Proc. Intl. Reliab. Phys. Symp. 2018 pp. 4F.4–1–6.

[3] C.-K. Hu, L. Gignac, G. Lian, C. Cabral, K. Motoyama, H. Shobha, J. Demarest, Y. Ostrovski, C.M. Breslin, M. Ali, J. Benedict, P.S. McLaughlin, J. Ni, X.H. Liu, Mechanisms of electromigration damage in Cu interconnects, Proc. Intl. Electron Devices Meeting, 2018, pp. 5.2.1–5.2.4.

[4] M.E. Sarychev, Y.V. Zhitnikov, General model for mechanical stress evolution during electromigration, J. Appl. Phys. 86 (6) (1999) 3068–3075.

[5] H. Ceric, S. Selberherr, Electromigration in submicron interconnect features of integrated circuits, Mater. Sci. Eng. R 71 (2011) 53–86.

[6] M.A. Korhonen, P. Børgesen, K.N. Tu, C.-Y. Li, Stress evolution due to electromigration in confined metal lines, J. Appl. Phys. 73 (8) (1993) 3790–3799.

[7] H. Zahedmanesh, P.R. Besser, C.J. Wilson, K. Croes, Airgaps in nano-interconnects: mechanics and impact on electromigration, J. Appl. Phys. 120 (2016) pp. 095 103–1–13.

[8] C.S. Smith, Grain shapes and other metallurgical applications of topology, Metallogr. Microstruct. Anal. 4 (1952) 543–567.

[9] L.E. Spinella, The Scaling and Microstructure Effects on the Thermal Stress and Reliability of Through-Silicon Vias in 3D Integrated Circuits, Dissertation The University of Texas at Austin, 2017.

[10] I. Ciofi, P.J. Roussel, Y. Saad, V. Moroz, C.-Y. Hu, R. Baert, K. Croes, A. Contino, K. Vandersmissen, W. Gao, P. Matagne, M. Badaroglu, C.J. Wilson, D. Mocuta, Z. Tőkei, Modeling of via resistance for advanced technology nodes, IEEE Trans. Electron Devices 64 (5) (2017) 2306–2313.

[11] R.S. Sorbello, Microscopic driving forces for electromigration, in: J.R. Lloyd, F.G. Yost, P.S. Ho (Eds.), Materials Reliability Issues in Microelectronics, 225 1996, pp. 3–10.

[12] H. Ceric, R.L. de Orio, J. Cervenka, S. Selberherr, A comprehensive TCAD approach for assessing electromigration reliability of modern interconnects, IEEE Trans. Device Mater. Reliab. 9 (1) (2009) 9–19.

[13] O.V. Pedreira, K. Croes, H. Zahedmanesh, K. Vandersmissen, M. van der Veen, V.V. Gonzalez, D. Dictus, L. Zhao, A. Kolies, Z. Tőkei, Electromigration and thermal storage study of barrierless co vias, Proc. Intl. Interconnect Technology Conf. 2018, pp. 48–50.

[14] S. Beyne, K. Paulussen, and H. Bender, "EM Activation Energy Variation with Line-Width: Grain Analysis," to be published.

[15] H. Mehrer, K. Klitzing, R. Merlin, H.-J. Queisser, B. Keimer (Eds.), Diffusion in Solids, Fundamentals, Methods, Materials, Diffusion-controlled Processes. Springer Series in Solid-State Sciences, 2007.

[16] C.-K. Hu, L. Gignac, R. Rosenberg, Electromigration of Cu/low dielectric constant interconnects, Microelectron. Reliab. 46 (2006) 213–231.

[17] Tan, Roy, Electromigration in ULSI interconnects, Materials Science and Engineering R 58 (2007) 1–75.

[18] COMSOL, Multiphysics, Version. 5.3a, (2017).

[19] R.W. Balluffi, Grain boundary diffusion mechanisms in metals, Metall. Trans. A. 13 (1982) 2069–2095.